Minimum-Variance Control Allocation Considering Parametric Model Uncertainty

Jared A. Grauer* and Jing Pei†
NASA Langley Research Center, Hampton, Virginia, 23681

The control allocation problem was investigated for linear dynamical systems with known parametric uncertainty. Minimizing a cost function that penalizes the variance of the error in achieving commanded forces and moments on the vehicle resulted in a special case of the weighted pseudo-inverse allocator. Rather than an engineer designing the weighting matrix, it is computed from the covariances of the control effectiveness parameters. This minimum-variance allocator balances the effectiveness of the control inputs against the corresponding levels of uncertainty. The approach was demonstrated using simulations of aircraft with realistic uncertainty levels operating in open-loop and closed-loop configurations. Results showed that when model uncertainty is known, significant, and unevenly distributed amongst the controls, the minimum-variance allocator more often achieves the intended steady-state forces and moments on the vehicle in comparison to other allocators, which can lead to increased performance, reliability, and safety during flight tests. The cost for this robustness is a diminished achievable moment space for the vehicle.

Nomenclature

$\mathbf{B}$	=	control input matrix
$\mathbb{E}$	=	expectation operator
$\mathbb{I}$	=	identity matrix
$J(\mathbf{u})$	=	cost function
L, M, N	=	body-axis moments, ft-lbf
n	=	number of variables
$\mathbf{S}$, $\mathbf{W}$	=	weighting matrices
s	=	Laplace variable
t	=	time, s
δ	=	control surface deflections, rad
$\boldsymbol{\theta}$	=	parameter estimates
σ	=	standard deviation or standard error
$\boldsymbol{\tau}$	=	generalized forces
$\lvert . \rvert$	=	determinant or absolute value

Superscripts

$\dot{}$	=	time derivative
$\hat{}$	=	estimated value
$\tilde{}$	=	error value
$^{-1}$	=	matrix inverse
^{T}	=	transpose

*Research Engineer, Dynamic Systems and Control Branch, MS 308. Associate Fellow AIAA.
†Aerospace Engineer, Atmospheric Flight Entry Systems Branch, MS 451. Member AIAA.

I. Introduction

When flight vehicles have redundant control effectors, control allocation is needed to distribute commands to individual actuators. A simple example is the mechanical ganging of individual left and right aileron surfaces to deflect in an anti-symmetric fashion and create a roll moment on an airplane. Other examples include fixed-wing aircraft with more than three control surfaces [1–4], multicopters and compound rotorcraft [5–7], launch vehicles with multiple gimbaled nozzles [8], and spacecraft with multiple reaction control jets [9, 10]. In these cases, control allocation can be used to simplify a vehicle design, increase control authority or reduce actuation requirements, optimize some aspect of the performance, or improve safety through redundancy and fault-tolerant designs [11–13].

Many approaches for control allocation have been developed, evaluated, and compared [5, 14–21]. With relatively few exceptions, such as Refs. [22–25], the allocator design is based on linear models, and robustness to modeling errors is evaluated using a nonlinear model and Monte Carlo simulations with different realizations of the model parameters. Parametric error can be important in control allocation design because this type of error creates unintended forces and moments on the vehicle which must then be suppressed by the pilot and/or a flight control system. Significant errors can lead to increased pilot workload and less desirable handling quality ratings, and can degrade closed-loop performance, lower robustness and control authority, increase control activity, create cross-axis coupling, introduce nonlinearities or aeroelastic responses, and shorten mission durations or actuator lifecycles [2, 15, 19].

As new vehicle configurations are developed, the problem of designing allocators for uncertain dynamic models could become more important. Some applications include urban air mobility vehicles with redundant rotors, aeroelastic airplanes with multiple trailing edge control surfaces, and lunar landers with many reaction control jets. In these cases, a design approach that directly considers the model uncertainty would help to improve robustness, performance, and safety. Some works have used robust control techniques to minimize the effects of bounded disturbances in the allocation problem [26–29]. Other works have used adaptive control techniques to evolve allocation law parameters and mitigate uncertainties in the plant model [30–32]. However, there seem to be few other significant works in the literature that directly address parametric uncertainty in the vehicle dynamic model for control allocation design.

In this work, an allocator was sought that would most likely produce the intended forces and moments on the vehicle, given a dynamic model and its parametric uncertainty. This uncertainty was quantified by the parameter covariance matrix, which may result from the Cramér-Rao bounds in a system identification analysis [33] or from dispersion models developed from uncertainty quantification or historical data. A cost function was formed based on the variances of the force and moment errors. Minimization of the cost function resulted in a linear allocator, which was found to be a special case of the well-known weighted pseudo-inverse allocator [21]. This *minimum-variance* solution is the most likely to produce the intended forces and moments and provides the optimal balance between effectiveness of and uncertainty in the control effectors. Calculation of the allocation law is standard and computationally simple, and could be done online to adapt to a real-time system identification analysis [33, 34].

The remaining paper is organized as follows. Section II defines the control allocation problem. Section III summarizes the weighted pseudo-inverse allocator to provide context for Section IV, which develops the minimum-variance allocator. Section V presents two examples to demonstrate minimum-variance control allocation. The first example is for the open-loop pitch dynamics of an airplane with two control effectors, and the second example is for the lateral-directional dynamics of an airplane operating with feedback control. Section VI concludes the paper.

II. Problem Statement

The equations of motion for a flight vehicle can often be written in the nonlinear form

$$\dot{\mathbf{x}} = \mathbf{f}(\mathbf{x}) + \boldsymbol{\tau}(\mathbf{u}) \tag{1}$$

where $\mathbf{x}$ is the $(n_x \times 1)$ state vector, $\mathbf{u}$ is the $(n_u \times 1)$ control input vector, and $\mathbf{f}$ and $\boldsymbol{\tau}$ are generalized forces arising from the states and controls, respectively. In the case where the controls appear linearly in the equations of motion, the last term in Eq. (1) simplifies to

$$\boldsymbol{\tau}(\mathbf{u}) = \mathbf{B}\mathbf{u} \tag{2}$$

where $\mathbf{B}$ is the $(n_x \times n_u)$ control input matrix. For systems with redundant control effectors, $n_x < n_u$ and $\mathbf{B}$ is wider than it is tall.

Figure 1 shows a block diagram of a generic flight control system. Based on inputs from a pilot and measurements from sensors, the control law commands a set of generalized forces $\boldsymbol{\tau}_c$ to be imparted on the vehicle. The commanded and actual generalized forces, $\boldsymbol{\tau}_c$ and $\boldsymbol{\tau}$ respectively, may differ due to parametric uncertainty, unmodeled dynamics,

linearization errors, and other factors. If present, the control allocator distributes those commands among the available control effectors. Control inputs drive the actuators, which create forces and moments that impact the aircraft motion. The control allocation problem concerns designing the allocator to compute $\mathbf{u}$ from $\boldsymbol{\tau}_c$.

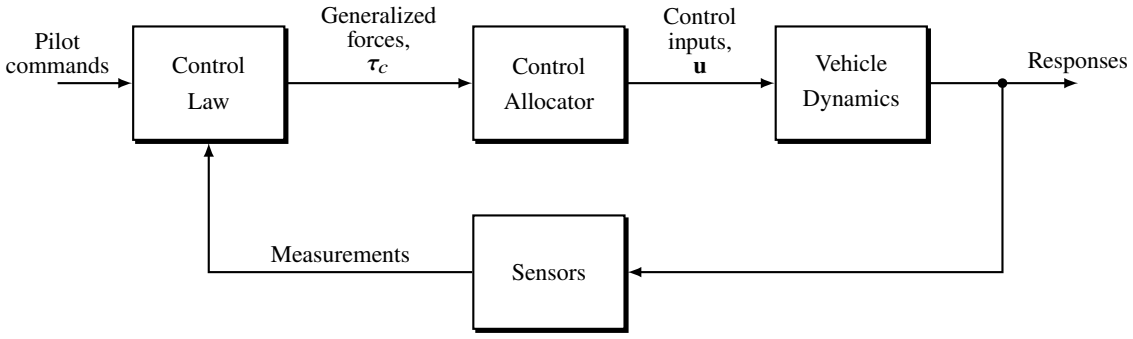


Fig. 1 Block diagram of the closed-loop vehicle system.

III. Weighted Pseudo-Inverse Allocator

This section summarizes the weighted pseudo-inverse (WPI) allocator. The minimum-variance allocator discussed next in Section IV is shown to be a special case of this allocator. For more details about the WPI allocator, see Ref. [21].

The WPI allocator is the solution that minimizes the cost function

$$J(\mathbf{u}) = \frac{1}{2}\mathbf{u}^T \mathbf{W}\mathbf{u} \tag{3}$$

subject to the constraint

$$\boldsymbol{\tau} = \mathbf{B}\mathbf{u} \tag{4}$$

A quadratic cost function, such as Eq. (3), is useful for minimizing the overall control activity. Equation (4) is needed to reduce the dimensionality of the problem and to relate the control inputs to the generalized forces acting on the vehicle. Note that this formulation considers the continuous, linear control allocation problem with symmetric, independent, and linear constraints.

In Eq. (3), $\mathbf{W}$ is an $(n_u \times n_u)$ positive semi-definite matrix that is designed to weight the relative use of some control effectors over others. For intuition and simplicity, $\mathbf{W}$ is usually chosen as a diagonal matrix. Bryson's rule can be used to select the diagonal elements according to the position or rate limits of the effectors [35]. According to Ref. [21], there is not much physical connection to off-diagonal weights or negative values, although these elements may be important when the control effectors or constraints are coupled. If some form of fault detection is present, specific elements can be set to zero to stop using a failed effector [11, 12]. If $\mathbf{W}$ is chosen as the identity matrix, meaning the control effectors are weighted equally, the solution reduces to the pseudo-inverse (PI) allocator (not to be confused with the acronym for proportional-integral control).

The WPI problem can be solved using the method of Lagrange multipliers by first forming the Lagrangian function [35, 36] as

$$\mathcal{L}(\mathbf{u}, \boldsymbol{\lambda}) = \frac{1}{2}\mathbf{u}^T \mathbf{W}\mathbf{u} + \boldsymbol{\lambda}^T \left(\boldsymbol{\tau}_c - \mathbf{B}\mathbf{u}\right) \tag{5}$$

where $\boldsymbol{\lambda}$ is the $(n_x \times 1)$ vector of Lagrange multipliers. Next, set the gradients of the Lagrangian

$$\frac{\partial \mathcal{L}}{\partial \mathbf{u}} = \mathbf{u}^T \mathbf{W} - \boldsymbol{\lambda}^T \mathbf{B} \tag{6a}$$

$$\frac{\partial \mathcal{L}}{\partial \boldsymbol{\lambda}} = \left(\boldsymbol{\tau}_c - \mathbf{B}\mathbf{u}\right)^T \tag{6b}$$

equal to zero. Finally, solve the resulting system of equations

$$\begin{bmatrix} \mathbf{W} & -\mathbf{B}^T \\ \mathbf{B} & \mathbf{0} \end{bmatrix} \begin{bmatrix} \mathbf{u} \\ \boldsymbol{\lambda} \end{bmatrix} = \begin{bmatrix} \mathbf{0} \\ \boldsymbol{\tau}_c \end{bmatrix} \tag{7}$$

for the allocation law as

$$\mathbf{u} = \mathbf{P}\,\boldsymbol{\tau}_c \tag{8}$$

by eliminating the Lagrange multipliers, where

$$\mathbf{P} = \mathbf{W}^{-1}\mathbf{B}^T\left(\mathbf{B}\,\mathbf{W}^{-1}\mathbf{B}^T\right)^{-1} \tag{9}$$

is the $(n_u \times n_x)$ allocation gain matrix.

The matrix multiplication in Eq. (9), analogous to the weighted least-squares solution, is computationally simple and can be implemented online during operation if needed. Note that when $\mathbf{B}$ is known without error, substituting Eqs. (8) and (9) into Eq. (2) reduces the generalized forces to those exactly desired by the control law, $\boldsymbol{\tau} = \boldsymbol{\tau}_c$.

IV. Minimum-Variance Allocator

The system dynamics in Eqs. (1) and (2) represent an approximate model of a physical system. This model contains several sources of error, including uncertainty in the values of parameters within the model. When the model is used to design an allocation law, the control inputs then also contain errors that produce unintended motions of the aircraft, which further burdens the pilot or control system.

Instead of minimizing the norm of the control input, as in Section III, the allocator could be designed to minimize the variance of the error in the generalized forces produced for a given model and its parametric uncertainty. This choice reduces the probability of generating unintended forces and moments on the vehicle.

To develop such an allocator, first define the generalized force error as

$$\tilde{\boldsymbol{\tau}} = \hat{\boldsymbol{\tau}} - \boldsymbol{\tau} \tag{10}$$

Here the notation has been made more specific so that now $\hat{\boldsymbol{\tau}}$ is the generalized force predicted by the model and $\boldsymbol{\tau}$ is the actual generalized force imparted on the vehicle. Next, choose the cost function to be minimized as

$$J(\mathbf{u}) = \frac{1}{2}\mathbb{E}\left[\tilde{\boldsymbol{\tau}}^T\mathbf{S}\,\tilde{\boldsymbol{\tau}}\right] \tag{11}$$

where $\mathbb{E}$ is the expectation operator and $\mathbf{S}$ is any $(n_x \times n_x)$ positive semi-definite matrix. For the simplest case where $\mathbf{S} = \mathbb{I}$, the cost function in Eq. (11) penalizes the sum of the diagonal elements in the allocation error covariance matrix, which is equivalent to the length of the generalized force error vector. Another case, where $\mathbf{S}$ is chosen using the relevant elements of the inertia tensor, is also considered later in Section V.B.

This problem formulation constitutes the minimum-variance (MV) control allocator. It is constructed under similar reasoning as the minimum-variance regulator [37] and minimum-variance state estimators, such as the Kalman filter [38, 39]. However, for the MV regulator and state estimator, the system is assumed to be known and the signals are uncertain whereas for the MV allocator problem considered here, the signals are known and the system is uncertain. Another difference is that the left generalized inverse is used in the estimation applications, whereas the right generalized inverse is used in control allocation.

Suppose that the control input matrix has a known functional dependence $\mathbf{B}(\boldsymbol{\theta})$ where $\boldsymbol{\theta}$ is an $(n_\theta \times 1)$ vector of parameters. For example in aircraft flight dynamics, the parameters could be dimensional or nondimensional control derivatives [33, 40]. Denote the (mean) parameter estimates as $\hat{\boldsymbol{\theta}}$ and quantify their uncertainty with the $(n_\theta \times n_\theta)$ covariance matrix $\mathbb{E}[\hat{\boldsymbol{\theta}}\hat{\boldsymbol{\theta}}^T]$. Equation (10) can then be expanded as

$$\tilde{\boldsymbol{\tau}} = \mathbf{B}(\hat{\boldsymbol{\theta}})\mathbf{u} - \mathbf{B}(\boldsymbol{\theta})\mathbf{u} \tag{12a}$$

$$= \left[\mathbf{B}(\hat{\boldsymbol{\theta}}) - \mathbf{B}(\boldsymbol{\theta})\right]\mathbf{u} \tag{12b}$$

Substituting this result into the cost function from Eq. (11) yields

$$J(\mathbf{u}) = \frac{1}{2}\mathbb{E}\left[\tilde{\boldsymbol{\tau}}^T\mathbf{S}\,\tilde{\boldsymbol{\tau}}\right] \tag{13a}$$

$$= \frac{1}{2}\mathbb{E}\left\{\mathbf{u}^T\left[\mathbf{B}^T(\hat{\boldsymbol{\theta}}) - \mathbf{B}^T(\boldsymbol{\theta})\right]\mathbf{S}\left[\mathbf{B}(\hat{\boldsymbol{\theta}}) - \mathbf{B}(\boldsymbol{\theta})\right]\mathbf{u}\right\} \tag{13b}$$

$$= \frac{1}{2}\mathbf{u}^T\mathbf{W}\mathbf{u} \tag{13c}$$

where the weighting matrix here becomes

$$\mathbf{W} = \mathbb{E}\left[\mathbf{B}^T(\hat{\boldsymbol{\theta}})\,\mathbf{S}\,\mathbf{B}(\hat{\boldsymbol{\theta}})\right] \tag{14a}$$

$$= \sum_{i=1}^{n_x}\sum_{j=1}^{n_x} s_{ij}\,\mathbb{E}\left[\mathbf{b}_i(\hat{\boldsymbol{\theta}})\,\mathbf{b}_j^T(\hat{\boldsymbol{\theta}})\right] \tag{14b}$$

In Eq. (14b), $\mathbf{b}_j^T$ is the jth row of $\mathbf{B}$ and s_{ij} is an element of $\mathbf{S}$. The term including the expectation operator is the covariance matrix of rows and columns of the control input matrix, which depends on the parameter uncertainties. To finish, the accompanying constraint for the optimization is

$$\boldsymbol{\tau}_c = \mathbb{E}\left[\mathbf{B}(\hat{\boldsymbol{\theta}})\,\mathbf{u}\right] \tag{15}$$

where the expectation operator is needed because $\hat{\boldsymbol{\theta}}$ is a random variable.

Because Eq. (13c) is of the same form as Eq. (3), the MV allocator is a special case of the WPI allocator for when the weighting matrix is selected as Eq. (14) and the constraint in Eq. (15) is used. For the MV allocator, the optimal weighting matrix is a linear combination of the covariance matrices for each row of $\mathbf{B}$ and is a function of the parameter uncertainties. This choice provides an optimal trade-off between the effectiveness of each control input and the uncertainty in that information.

The MV allocator reduces in some instances. In the limit where each effector is known with the same accuracy, the MV allocator reduces to the PI allocator. In the case that the covariance matrix used to design the allocator is not a true reflection of the uncertainty in the control input matrix, the allocator loses optimality and is no longer the minimum-variance allocator, but remains a WPI allocator. This sensitivity depends on the model parameter estimates and the inaccuracy in quantifying the associated covariance matrix, and should be examined for specific cases. Also note that the MV allocator is susceptible to the same undesirable characteristics of the WPI allocator, such as not directly taking into account actuator position or rate limits, although there are techniques to mitigate these shortcomings [21].

V. Examples

A. Single-Axis Open-Loop Example

For this first example, the simplest control allocation problem (involving two control effectors and one moment) was investigated. A longitudinal aircraft model identified from flight test data was used to design PI and MV allocators. A Monte Carlo simulation was then run where realizations of the "true" system dynamics were randomly varied according to the identified parameter covariance matrix while the steady-state error in achieving a unit pitching moment command was recorded. This process was repeated for three other cases that had variations in the control effectiveness and uncertainties in comparison to the baseline case. Results for these four cases are summarized in Table 1 and Fig. 3.

The basis for this example is the NASA T-2 airplane, which is pictured during flight in Fig. 2. The T-2 is a subscale transport-type aircraft with a 6.8 ft wingspan and 50 lbf weight [41]. Among its 16 control effectors are four independent trailing-edge control surfaces on the horizontal tail. During flight tests, these surfaces were at times moved as outboard and inboard elevator pairs, δ_{e_o} and δ_{e_i}, to produce two independent sources of pitching moments on the airplane.



Fig. 2 T-2 airplane in flight (credit: NASA Langley Research Center).

For this configuration, the contributions from the control surfaces to the pitching moment were modeled as

$$\tau = \mathbf{B}\mathbf{u} = \mathbf{b}_1^T \mathbf{u} = \begin{bmatrix} M_{\delta_{e_o}} & M_{\delta_{e_i}} \end{bmatrix} \begin{bmatrix} \delta_{e_o} \\ \delta_{e_i} \end{bmatrix} \tag{16}$$

where the uncertain model parameters were the dimensional control derivatives $M_{\delta_{e_o}}$ and $M_{\delta_{e_i}}$. These parameters were estimated from flight test data, where the T-2 was perturbed about straight and level flight with excitation inputs, using the equation-error method with Fourier transform data [33]. The first two rows of Table 1 list these identified estimates and uncertainties under the column for Case 1. Figure 3(a) also shows this information graphically, where the dot is the mean estimate and the ellipse represents the 95% confidence bound (two standard errors). The 38 deg rotation of the ellipse relative to the coordinate axes is due to the covariance of 0.201 between the two control derivatives. The estimates and uncertainties for each of the elevator pairs were approximately equal. Furthermore, the uncertainties were relatively small, at about 4% of the estimated parameter values.

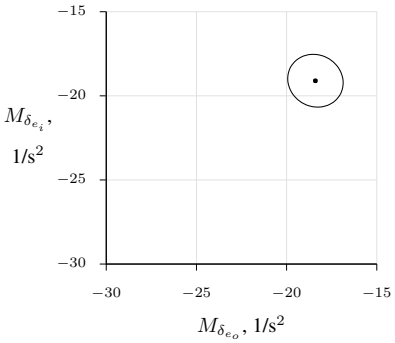
Table 1 Summary of numerical values used in the T-2 example.

Parameter	Case 1	Case 2	Case 3	Case 4
$\hat{\boldsymbol{\theta}}$	$\begin{bmatrix} -18.4 & -19.1 \end{bmatrix}^T$	$\begin{bmatrix} -18.4 & -19.1 \end{bmatrix}^T$	$\begin{bmatrix} -18.4 & -22.9 \end{bmatrix}^T$	$\begin{bmatrix} -18.4 & -22.9 \end{bmatrix}^T$
$\mathbb{E}\left[\hat{\boldsymbol{\theta}}\hat{\boldsymbol{\theta}}^T\right]$	$\begin{bmatrix} 0.553 & 0.201 \\ 0.201 & 0.653 \end{bmatrix}$	$\begin{bmatrix} 0.553 & 0.201 \\ 0.201 & 2.61 \end{bmatrix}$	$\begin{bmatrix} 0.553 & 0.201 \\ 0.201 & 2.61 \end{bmatrix}$	$\begin{bmatrix} 2.21 & 0.201 \\ 0.201 & 0.653 \end{bmatrix}$
$\mathbf{P}_{PI}$	$\begin{bmatrix} -0.0262 \\ -0.0272 \end{bmatrix}$	$\begin{bmatrix} -0.0262 \\ -0.0272 \end{bmatrix}$	$\begin{bmatrix} -0.0214 \\ -0.0266 \end{bmatrix}$	$\begin{bmatrix} -0.0214 \\ -0.0266 \end{bmatrix}$
$\mathbf{P}_{MV}$	$\begin{bmatrix} -0.0291 \\ -0.0244 \end{bmatrix}$	$\begin{bmatrix} -0.0469 \\ -0.0073 \end{bmatrix}$	$\begin{bmatrix} -0.0433 \\ -0.0089 \end{bmatrix}$	$\begin{bmatrix} -0.0061 \\ -0.0388 \end{bmatrix}$
$\sigma(\tilde{\tau}_{PI})$, ft-lbf	0.0338	0.0508	0.0481	0.0409
$\sigma(\tilde{\tau}_{MV})$, ft-lbf	0.0338	0.0384	0.0378	0.0343

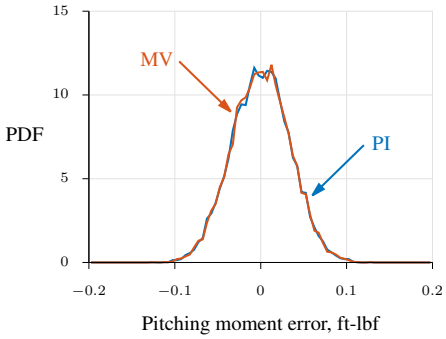
These estimates were used to design PI and MV allocators, allocation gain matrices for which are listed in the third and fourth rows of Table 1. As mentioned in Section III, the PI allocator is a simplification of the WPI allocator where $\mathbf{W} = \mathbb{I}$. For the MV allocator, the matrix $\mathbf{S} = \mathbb{I}$ was used. Because in this example the model parameters are directly elements of the control input matrix, $\mathbf{B}(\boldsymbol{\theta}) = \boldsymbol{\theta}^T$, the weighting matrix reduced to $\mathbf{W} = \mathbb{E}[\hat{\boldsymbol{\theta}}\hat{\boldsymbol{\theta}}^T]$.

To investigate the effect of the allocator designs on the accuracy of the steady-state pitching moment produced, 10,000 simulation runs were performed. In each run, a unit pitching moment was commanded of the two allocators. The resulting pitching moments predicted by the allocators were compared against outputs from the "true" simulated plant model, which was randomly drawn from a Gaussian distribution having the covariance matrix listed in the second row of Table 1 [39].

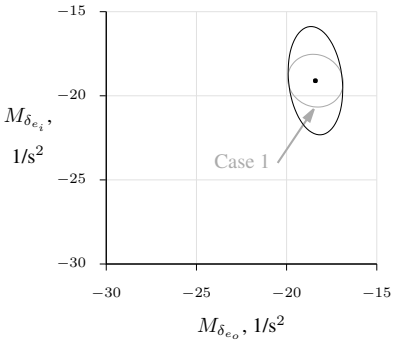
Figure 3(b) shows a probability density function (PDF) estimate for the pitching moment errors over the 10,000 simulation runs. The bin sizes were 0.005 ft-lbf in width and were taken between −0.2 and 0.2 ft-lbf. In general, a lower variance is indicated by a thinner and taller PDF. This information is also listed as the fifth and sixth rows of Table 1 as standard deviations of error. In this case, the PI allocator and the MV allocator both had approximately the same allocation gain matrices and an error standard deviation of 0.0338 ft-lbf. This was because the effectiveness and uncertainty of the control surfaces were approximately equal and so the MV allocator essentially reduced to the PI allocator. This will not be the situation for the next three cases, where the model parameters and uncertainties are different between the two control effectors.



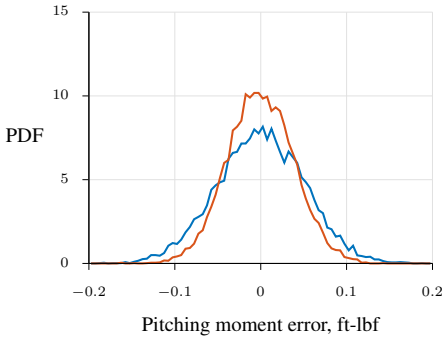
(a) Case 1 parameters and 2σ bounds.



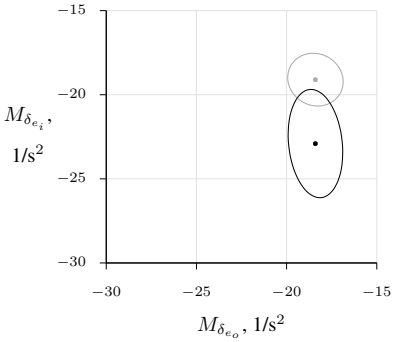
(b) Case 1 pitching moment error histogram.



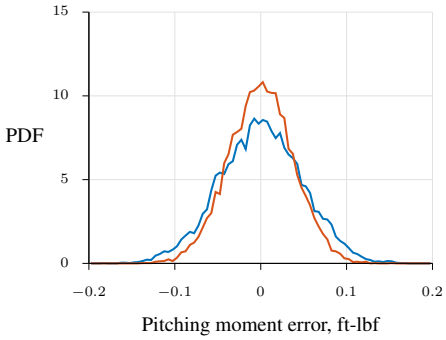
(c) Case 2 parameters and 2σ bounds.



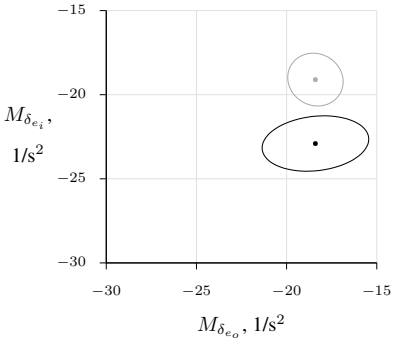
(d) Case 2 pitching moment error histogram.



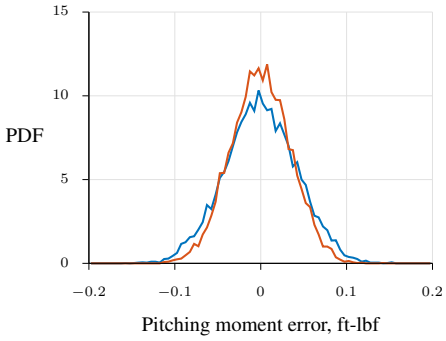
(e) Case 3 parameters and 2σ bounds.



(f) Case 3 pitching moment error histogram.



(g) Case 4 parameters and 2σ bounds.



(h) Case 4 pitching moment error histogram.

Fig. 3 T-2 example results for 10,000 runs.

In a second case, the control derivatives remained the same but the baseline standard error for $M_{\delta_{e_i}}$ was increased by a factor of two. Table 1 lists these values under the column for Case 2 and Fig. 3(c) shows this information visually. For reference, the baseline estimates from Case 1 are also shown in gray. The PI allocator gain matrix did not change from Case 1 because the mean estimates were the same, the but MV allocation matrix used δ_{e_o} more heavily than δ_{e_i} because of the change in the uncertainties. Figure 3(d) shows the PDF from running another 10,000 Monte Carlo simulations for the new values in Case 2. In comparison to the PI allocator, the MV allocator had 24% less error standard deviation.

In the third case, the standard error of $M_{\delta_{e_i}}$ was again increased by a factor of two relative to Case 1 and also the effectiveness $M_{\delta_{e_i}}$ was increased by 20%. Table 1 lists these values under the column for Case 3 and Fig. 3(e) shows this information visually. The PI allocation gain matrix weighted δ_{e_i} more heavily than δ_{e_o} because of the greater control effectiveness. On the contrary, the MV allocator weighted δ_{e_o} more heavily than δ_{e_i} because although the δ_{e_i} was the stronger control, its effectiveness was known less accurately. Figure 3(f) shows the resulting PDF of errors from running another 10,000 Monte Carlo simulations. The MV allocator had a lower pitching moment error standard deviation by 21% in comparison to the PI allocator.

In the fourth case, the baseline effectiveness of $M_{\delta_{e_i}}$ was again increased 20% relative to Case 1 and also the standard error of $M_{\delta_{e_o}}$ was increased by a factor of two. Table 1 lists these values under the column for Case 4 and Fig. 3(g) shows this information visually. This scenario is typical, where the most effective control inputs are measured or known with the highest amount of accuracy. The PI allocation gain matrix did not change from Case 3 because the model parameter estimates did not change in value. The MV allocation gain matrix weighted δ_{e_i} more heavily because this input was both more effective and had less uncertainty than δ_{e_o}. Figure 3(h) shows the PDF of pitching moment errors from another 10,000 simulation runs. The MV allocator had a lower pitching moment error standard deviation by 16% in comparison to the PI allocator.

In each of these four cases with the T-2 longitudinal model, the MV allocator produced the same or lower amount of pitching moment error than the PI allocator. The amount of performance increase for the MV allocator depended on the relative differences of the model parameters and the associated uncertainties, as these quantities factor into the allocation matrix calculation.

B. Multiple-Axis Closed-Loop Example

This example investigates the effect of parametric uncertainty and allocator design on the closed-loop dynamics of the F-16 Advanced Fighter Technology Integration (AFTI) aircraft model. Figure 4 shows a photograph of the airplane in flight. The F-16 AFTI had a 30 ft wingspan and an approximate weight of 21,000 lbf. For control of the lateral-directional dynamics, the airplane had antisymmetric ailerons δ_a, differential stabilator δ_{ds}, rudder δ_r, and vertical canards δ_{vc} mounted underneath the engine intake.



Fig. 4 F-16 AFTI airplane in flight (credit: NASA).

Reference [42] provides linear models of the aircraft bare-airframe dynamics. The model for the lateral-directional

dynamics in straight and level flight at 0.6 Mach and 30,000 ft was

$$\begin{bmatrix} \dot{\beta} \\ \dot{p} \\ \dot{r} \\ \dot{\phi} \end{bmatrix} = \begin{bmatrix} -0.154 & 0.0824 & -0.998 & 0.0521 \\ -19.2 & -0.894 & 0.319 & 0 \\ 2.30 & -0.0009 & -0.279 & 0 \\ 0 & 1 & 0.0823 & 0 \end{bmatrix} \begin{bmatrix} \beta \\ p \\ r \\ \phi \end{bmatrix} + \begin{bmatrix} 0.0004 & 0.0144 & 0.0212 & 0.0074 \\ -17.5 & -13.6 & 3.92 & 0.415 \\ -0.268 & -1.51 & -1.97 & 1.51 \\ 0 & 0 & 0 & 0 \end{bmatrix} \begin{bmatrix} \delta_a \\ \delta_{ds} \\ \delta_r \\ \delta_{vc} \end{bmatrix} \quad (17)$$

where the states are perturbations in the sideslip angle β, roll rate p, yaw rate r, and roll angle ϕ. Modal characteristics for this model are listed in the first row of Table 2. A shorthand notation [40] is used to write the negative root of a first-order pole in parentheses, or alternatively the damping ratio and natural frequency of a second-order pole in brackets. The control surface position and rate limits from Ref. [42] are given in Table 3. Actuator models were included as first-order systems with a 0.05 s lag [1, 43].

Table 2 F-16 rigid-body modal characteristics.

	Spiral	Dutch roll	Roll
Bare airframe	(0.0733)	[0.110, 1.96]	(0.821)
Closed-loop design	(0.0262)	[0.437, 1.63]	(1.15)
PI	(0.0296 ± 0.0024)*	[0.465 ± 0.0232, 1.59 ± 0.0377]	(1.10 ± 0.0471)
WPI	(0.0297 ± 0.0026)	[0.466 ± 0.0254, 1.58 ± 0.0363]	(1.10 ± 0.0450)
MV1	(0.0298 ± 0.0030)	[0.473 ± 0.0465, 1.60 ± 0.0597]	(1.09 ± 0.0348)
MV2	(0.0296 ± 0.0017)	[0.470 ± 0.0268, 1.59 ± 0.0350]	(1.09 ± 0.0396)

*Values represent the mean and standard deviation.

Table 3 F-16 control surface position and rate limits.

Control surface	Position limit, deg	Rate limit, deg/s
Ailerons	±20	52
Stabilators	±25	60
Rudder	±30	120
Vertical canards	±27	100

To improve the dynamics for the pilot, a simple stability augmentation system (SAS) was designed using feedback from the roll rate and yaw rate. Figure 5 shows a block diagram of the closed-loop system. The pilot lateral stick δ_{lat} and pedal δ_{ped} inputs are combined with the feedback to command the virtual aileron δ_{va_c} and virtual rudder δ_{vr_c}. These commands are then passed through the allocator to the four individual actuators. The allocator was designed to output control surface commands, rather than moments, to facilitate a more conventional SAS design. No other elements of a control system were included. The feedback gains and washout filter were iteratively tuned using the root locus technique to agree with industry-standard handling qualities guidelines [44]. The resulting modal characteristics for the closed-loop system are listed in the second row of Table 2. The main effects of the feedback were to increase the Dutch roll mode damping ratio and increase the roll mode time constant.

Table 4 lists the control derivative uncertainties assumed for this example. The primed notation indicates that the inertial coupling has been applied to the roll and yaw axes [40]. The values shown reflect the standard errors and are given as percentages of the corresponding control derivatives. Typical of fixed-wing aircraft, the on-axis terms (for example, roll moment due to aileron deflection) are known with less uncertainty than the off-axis terms (for example, yaw moment due to aileron deflection). The covariance matrix for the control derivatives was assumed to be diagonal with covariances among pairs of effectors neglected.

Four different allocators were designed to convert virtual aileron and rudder commands to actuator commands. Only the moment equations, corresponding to the second and third rows of Eq. (17), were used; side force was not directly commanded. The first allocator was a PI design. The second allocator was a WPI design where Bryson's rule was used

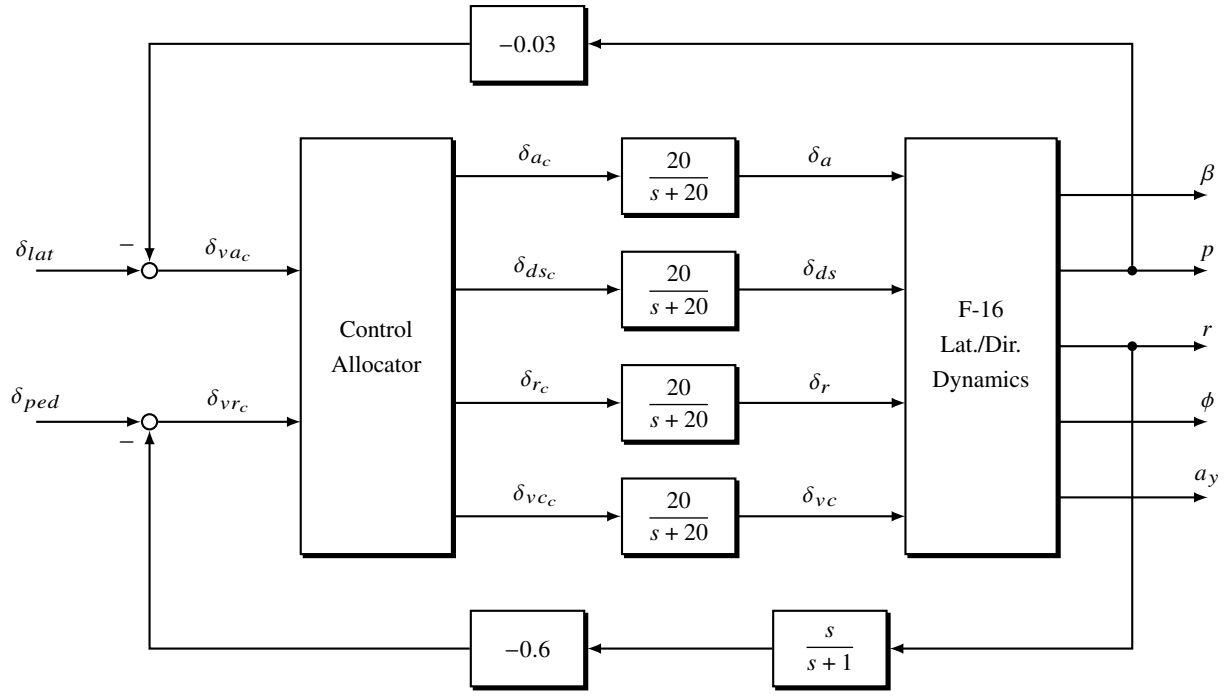


Fig. 5 Block diagram of F-16 AFTI stability augmentation system.

Table 4 F-16 control effectiveness standard errors.

Force or moment	δ_a	δ_{ds}	δ_r	δ_{vc}
Y	50%	50%	5%	10%
L'	5%	10%	20%	25%
N'	50%	50%	5%	10%

to choose the weighting matrix as

$$\mathbf{W} = \begin{bmatrix} 0.05 & 0 & 0 & 0 \\ 0 & 0.04 & 0 & 0 \\ 0 & 0 & 0.03 & 0 \\ 0 & 0 & 0 & 0.04 \end{bmatrix} \tag{18}$$

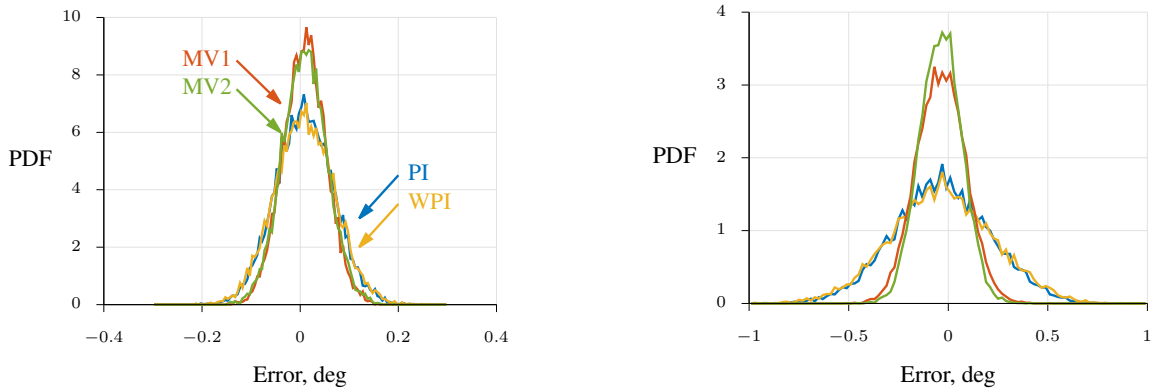
based on the ranges of the control surfaces given in Table 3. The third design, denoted "MV1," was a minimum-variance allocator with $\mathbf{S} = \mathbb{I}$. The fourth design, denoted "MV2," was another minimum-variance allocator where $\mathbf{S}$ was instead chosen as the relevant moments and products of inertia

$$\mathbf{S} = \begin{bmatrix} I_{xx} & -I_{xz} \\ -I_{xz} & I_{zz} \end{bmatrix} = \begin{bmatrix} 10,033 & -282 \\ -282 & 61,278 \end{bmatrix} \text{slug-ft}^2 \tag{19}$$

Similar to the T-2 example in Section V.A, Monte Carlo simulations were performed where for each run, a different realization of the control input matrix was drawn. The steady-state moment errors and the closed-loop dynamics using each of the four designed allocators were evaluated. Only the bare-airframe control input matrix was varied; the state matrix in Eq. (17), actuator dynamics, and elements of the control system were assumed to be known perfectly and were not varied. For each case, 1 deg of virtual aileron and 1 deg of virtual rudder were commanded from the pilot inputs.

Figure 6 shows error PDFs of the virtual aileron and rudder errors for 10,000 simulation runs. Figure 6(a) uses bins 0.005 deg in width between −0.3 and 0.3 deg, whereas Fig. 6(b) uses bins 0.02 deg in width between −1 and 1 deg.

The minimum-variance allocators had error standard deviations that were approximately 25% lower for the roll axis and 54% lower for the yaw axis as compared to the PI and WPI allocators. The MV2 allocator had a slightly lower standard deviation for the rudder error than the MV1 allocator. All allocators had small biases in the error distributions (under 1% for the virtual aileron and about 4% for the virtual rudder) due to side forces generated by the control surface deflections not considered during the allocator design.



(a) Virtual aileron error.

(b) Virtual rudder error.

Fig. 6 F-16 error histograms for 10,000 runs.

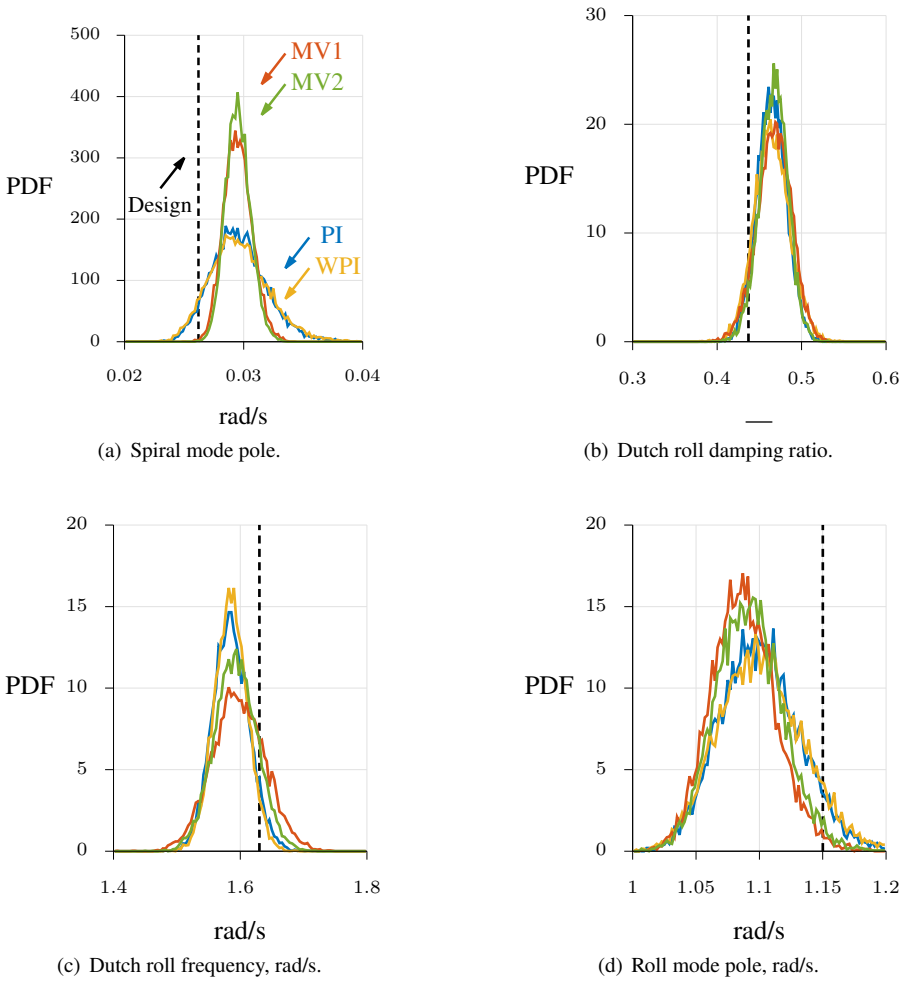
Although not directly optimized, the distributions of the resulting closed-loop modes using the four allocator designs were also examined. Modal characteristics for the 10,000 simulation runs are listed in the last four rows of Table 2 as mean values and standard deviations of the scatter. This same information is depicted visually as histograms in Fig. 7 and as poles on the complex plane in Fig. 8.

The mean values for the modal characteristics were approximately the same for all the allocators, and the mean values again had small biases (about 13% in the spiral pole, 7% in the dutch roll damping ratio, 2% in the dutch roll frequency, and 4% in the roll pole) due to the side force components neglected during the allocator design and the inclusion of actuator dynamics. These biases shift the distributions from the black dashed lines in Fig. 7 and the black x's in Fig. 8. In general, the MV2 had the lowest biases and standard deviations, particularly for the spiral and roll modes. Again, note that none of the allocators were optimized for achieving closed-loop dynamics.

Another aspect of the allocator performance is how large a "moment" space can be reached by the allocator design. The attainable moment set (AMS) is determined by the control input matrix and the control effector limits. The particular moment set (PMS) is determined additionally by the allocation law. The ratio of the volumes for these two sets η is a measure of efficiency for the allocator. For a perfect allocator, $\eta = 1$ and the PMS is equal to the AMS, meaning that any moment the aircraft is capable of generating can be achieved.

Figure 9 shows the moment sets for the F-16 model and each of the four allocators. The blue areas represent the AMS for one realization of the control input matrix, whereas the red areas (which are mostly encased by the AMS) represent the PMS. The PI and WPI allocators are comparatively more efficient than the MV allocators and fill more of the AMS. However, the PI and WPI allocators also have small regions of the PMS that extend beyond the AMS (shown in brighter red), meaning that the moments predicted by the model to be attainable cannot be generated. Attempting to operate in this part of the moment space will saturate the control surfaces and degrade the control performance. On the other hand, the MV allocators conservatively remain within the AMS, where the margins are dependent on the model uncertainty. However, the cost of this robustness is a 40%–50% degrade in efficiency of the allocator. In this case, a trade study is recommended to determine which allocator is best suited for the mission performance requirements.

Another metric to quantify actuator performance is to measure the deviation of $\mathbf{P}$ as a generalized inverse of $\mathbf{B}$. For a perfect linear allocator, $\mathbf{BP} = \mathbb{I}$. For the 10,000 simulation runs, the quantity $|\mathbf{BP} - \mathbb{I}|$ was recorded for each of the four allocators. The resulting mean values and standard deviations of scatter are listed in Table 5 for the four allocators. As expected, the minimum-variance allocators had lower mean values and standard deviations of this metric than the PI and WPI allocators.



(a) Spiral mode pole.

(b) Dutch roll damping ratio.

(c) Dutch roll frequency, rad/s.

(d) Roll mode pole, rad/s.

Fig. 7 F-16 histograms of closed-loop modal characteristics for 10,000 runs.

Table 5 F-16 deviation of P as a generalized inverse of B, listed as mean and standard deviations for 10,000 simulation runs.

Allocator	$\lvert \mathbf{BP} - \mathbb{I} \rvert$
PI	$18.4 \times 10^{-6} \pm 7.5 \times 10^{-3}$
WPI	$28.0 \times 10^{-6} \pm 6.5 \times 10^{-3}$
MV1	$17.4 \times 10^{-6} \pm 5.7 \times 10^{-3}$
MV2	$4.23 \times 10^{-6} \pm 3.7 \times 10^{-3}$

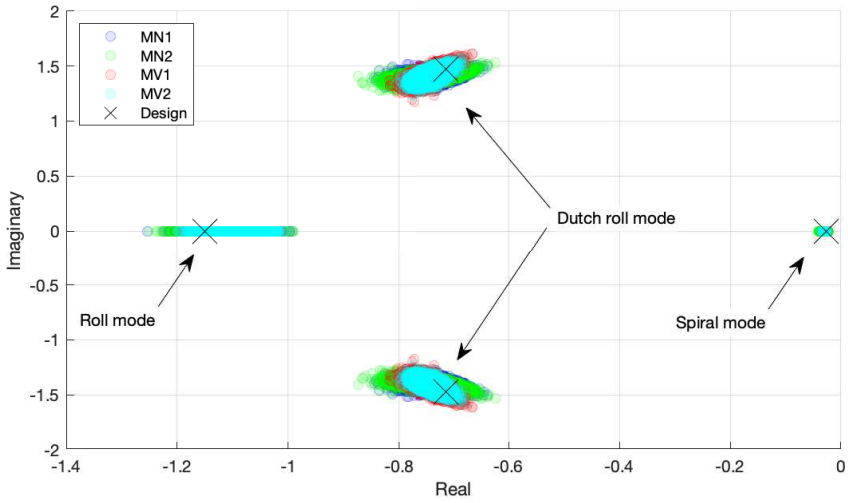
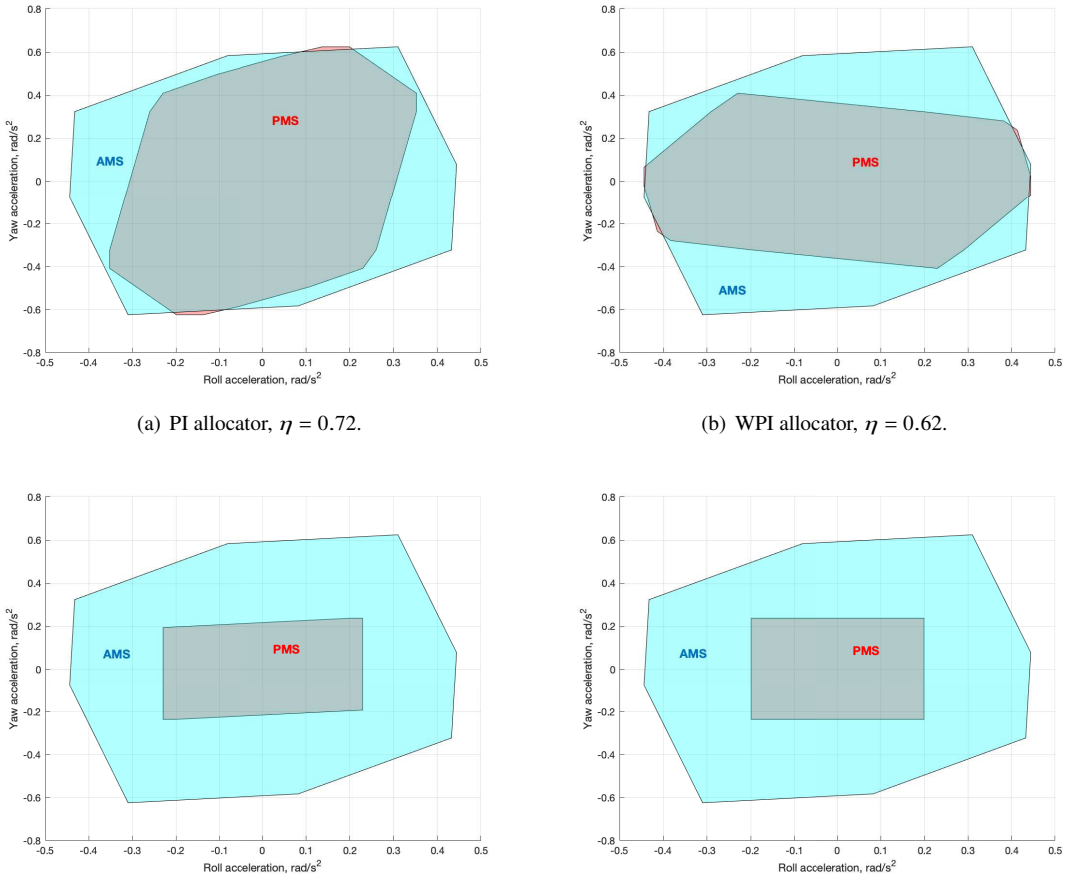


Fig. 8 F-16 closed-loop poles for 10,000 runs.



(a) PI allocator, $\eta = 0.72$.

(b) WPI allocator, $\eta = 0.62$.

(c) MV1 allocator, $\eta = 0.22$.

(d) MV2 allocator, $\eta = 0.21$.

Fig. 9 F-16 example attainable moment set (blue) and particular moment set (red) for one run.

VI. Conclusions

A minimum-variance control allocator was developed for dynamic systems that are linear in the control inputs and have parametric uncertainty. The minimum-variance allocator was found to be a special case of the commonly-used weighted pseudo-inverse allocator for when the weighting matrix is chosen as the covariance matrix of the control effectiveness parameters.

The allocator design and efficacy were demonstrated in two examples. The first example was the open-loop pitching moment from two elevator surface pairs for the NASA T-2 subscale airplane. The second example was the closed-loop lateral-directional dynamics from four control surfaces for the F-16 AFTI airplane. Simulations were run where the actual vehicle dynamics model was varied according to known uncertainties. In each example, the minimum-variance allocators more often achieved the desired steady-state forces and moments on the vehicle in comparison to allocators based on pseudo-inverse methods, as expected.

Minimum-variance control allocation is appropriate to use in situations where the uncertainties in the control effectiveness parameters are known, significant, and unequally distributed amongst the effectors. If the uncertainties are assumed incorrectly, the minimum-variance allocator can still improve robustness but is not optimal. In the cases where the uncertainties are insignificant or evenly distributed among the effectors, the minimum-variance allocator simplifies to the pseudo-inverse allocator. Otherwise, the minimum-variance allocator performs an optimal trade-off between the control effectiveness and the associated uncertainty to most likely produce the intended forces and moments on the vehicle and improve the overall performance. The cost for this robustness to parametric uncertainty using minimum-variance control allocation is decreased maneuverability resulting from a smaller achievable moment space. Some potential applications include flight tests of experimental aircraft, urban air mobility vehicles, and manned spacecraft. In these cases, vehicles typically have redundant control effectors and significant model uncertainty, and safety of flight is paramount.

Acknowledgments

This research was supported by the NASA Artemis program, under the Human Landing System (HLS) project. Previous support came from the NASA Aeronautics Research Mission Directorate (ARMD) Transformative Tools and Technologies (TTT) project, under the Autonomous Systems / Intelligent Contingency Management subproject. Technical discussions about this material with Michael Acheson, John Davidson, Eugene Morelli, Jeb Orr, and Robert Sanner are acknowledged and appreciated.

References

[1] Bosworth, J., "Linearized Aerodynamic and Control Law Models of the X-29A Airplane and Comparison With Flight Data," NASA TM-4356, Feb. 1992.

[2] Ngo, A., Reigelsperger, W., Banda, S., and Bessolo, J., "Multivariable Control Law Design for a Tailless Airplane," *Guidance, Navigation, and Control Conference*, AIAA Paper 96-3866, Jul. 1996. doi:10.2514/6.1996-3866.

[3] Ryan, J., Bosworth, J., Burken, J., and Suh, P., "Current and Future Research in Active Control of Lightweight, Flexible Structures Using the X-56 Aircraft," *Aerospace Sciences Meeting*, AIAA Paper 2014-0597, Jan. 2014. doi:10.2514/6.2014-0597.

[4] Niestroy, M., Dorsett, K., and Markstein, K., "A Tailless Fighter Aircraft Model for Control-Related Research and Development," *Modeling and Simulation Technologies Conference*, AIAA Paper 2017-1757, Jan. 2017. doi:10.2514/6.2017-1757.

[5] Ivler, C., and Juhasz, O., "Evaluation of Control Allocation Techniques for a Medium Lift Tilt-Rotor," *American Helicopter Society Annual Forum*, May 2015.

[6] Berger, T., Juhasz, O., Lopez, M., Tischler, M., and Horn, J., "Modeling and Control of Lift Offset Coaxial and Tiltrotor Rotorcraft," *European Rotorcraft Forum*, Paper 99, Sep. 2018. doi:10.1007/s13272-019-00414-0.

[7] Simmons, B., and Murphy, P., "Wind Tunnel-Based Aerodynamic Model Identification for a Tilt-Wing, Distributed Electric Propulsion Aircraft," *Atmospheric Flight Mechanics Conference*, AIAA Paper 2021-1298, Jan. 2021. doi:10.2514/6.2021-1298.

[8] Orr, J., and Slegers, N., "High-Efficiency Thrust Vector Control Allocation," *Journal of Guidance, Control, and Dynamics*, Vol. 37, No. 2, 2014, pp. 374–382. doi:10.2514/1.61644.

[9] Doman, D., Gamble, B., and Ngo, A., "Quantized Control Allocation of Reaction Control Jets and Aerodynamic Control Surfaces," *Journal of Guidance, Control, and Dynamics*, Vol. 33, No. 1, 2009, pp. 13–24. doi:10.2514/1.37312.

[10] Pei, J., Choueri, M., Elandt, R., Peck, M., and Finch, P., "An Innovative Control Allocation Scheme to Address Reaction Thruster Interactions on a 3U CubeSat," *Guidance, Navigation, and Control Conference and Exhibit*, AIAA Paper 2018-2096, Jan. 2018. doi:10.2514/6.2018-2096.

[11] Davidson, J., Lallman, F., and Bundick, W., "Real-Time Adaptive Control Allocation Applied to a High Performance Aircraft," *SIAM Conference on Control and its Applications*, Jul. 2000.

[12] Davidson, J., Lallman, F., and Bundick, W., "Integrated Reconfigurable Control Allocation," *Guidance, Navigation, and Control Conference*, AIAA Paper 2001-4083, Aug. 2001. doi:10.2514/6.2001-4083.

[13] Liu, Y., and Crespo, L., "Adaptive Control Allocation in the Presence of Actuator Failures," *Guidance, Navigation, and Control Conference*, AIAA Paper 2010-7772, Aug. 2010. doi:10.2514/6.2010-7772.

[14] Enns, D., "Control Allocation Approaches," *Guidance, Navigation, and Control Conference*, AIAA Paper 98-4109, Aug. 1998. doi:10.2514/6.1998-4109.

[15] Page, A., and Steinberg, M., "A Closed-Loop Comparison of Control Allocation Methods," *Guidance, Navigation, and Control Conference and Exhibit*, AIAA Paper 2000-4538, Aug. 2000. doi:10.2514/6.2000-4538.

[16] Page, A., and Steinberg, M., "High-Fidelity Simulation Testing of Control Allocation Methods," *Guidance, Navigation, and Control Conference and Exhibit*, AIAA Paper 2002-4547, Aug. 2002. doi:10.2514/6.2000-4547.

[17] Bodson, M., "Evaluation of Optimization Methods for Control Allocation," *Journal of Guidance, Control, and Dynamics*, Vol. 25, No. 4, 2002, pp. 703–711. doi:10.2514/2.4937.

[18] Oppenheimer, M., Doman, D., and Bolender, M., "Control Allocation for Over-actuated Systems," *Mediterranean Conference on Control and Automation*, Jun. 2006. doi:10.1109/MED.2006.328750.

[19] Ma, J., Li, P., Li, W., and Zheng, Z., "Performance Comparison of Control Allocation for Aircraft with Control Effectiveness Uncertainties," *Asia Simulation Conference — 7th International Conference on System Simulation and Scientific Computing*, IEEE Paper, pp. 164–169, Oct. 2008. doi:10.1109/ASC-ICSC.2008.4675349.

[20] Johansen, T., and Fossen, T., "Control Allocation — A Survey," *Automatica*, Vol. 49, 2013, pp. 1087–1103. doi:10.1016/j.automatica.2013.01.035.

[21] Durham, W., Bordignon, K., and Beck, R., *Aircraft Control Allocation*, Wiley, 2017, pp. 65–160. doi:10.1002/9781118827789.

[22] Doman, D., and Oppenheimer, M., "Improving Control Allocation Accuracy for Nonlinear Aircraft Dynamics," *Guidance, Navigation, and Control Conference*, AIAA Paper 2002-4667, Aug. 2002. doi:10.2514/6.2002-4667.

[23] Bolender, M., and Doman, D., "Nonlinear Control Allocation Using Piecewise Linear Functions," *Journal of Guidance, Control, and Dynamics*, Vol. 27, No. 6, 2004, pp. 1017–1027. doi:10.2514/1.9546.

[24] Bolender, M., and Doman, D., "Method for Determination of Nonlinear Attainable Moment Sets," *Journal of Guidance, Control, and Dynamics*, Vol. 27, No. 5, 2004, pp. 907–914. doi:10.2514/1.9548.

[25] Matamoros, I., and de Visser, C., "Incremental Nonlinear Control Allocation for a Tailless Aircraft with Innovative Control Effectors," *Guidance, Navigation, and Control Conference*, AIAA Paper 2018-1116, Jan. 2018. doi:10.2514/6.2018-1116.

[26] Cui, L., and Yang, Y., "Disturbance Rejection and Robust Least-Squares Control Allocation in Flight Control System," *Journal of Guidance, Control, and Dynamics*, Vol. 34, No. 6, 2011, pp. 1632–1643. doi:10.2514/1.52234.

[27] Choi, B., Kim, H., and Kim, Y., "Robust Control Allocation with Adaptive Backstepping Flight Control," *Journal of Aerospace Engineering*, Vol. 228, No. 7, 2014, pp. 1033–1046. doi:10.1177/0954410013483687.

[28] Duan, M., and Okwudire, C., "Proxy-Based Optimal Dynamic Control Allocation for Multi-Input Multi-Output Over-Actuated Systems," *Dynamic Systems and Control Conference*, ASME Paper DSCC2017-5343, Oct. 2017. doi:10.1115/DSCC2017-5343.

[29] Duan, M., and Okwudire, C., "Proxy-Based Optimal Control Allocation for Dual-Input Over-Actuated Systems," *IEEE/ASME Transactions on Mechatronics*, Vol. 23, No. 2, 2018, pp. 895–905. doi:10.1109/TMECH.2018.2796500.

[30] Schwager, M., Annaswamy, A., and Lavretsky, E., "Adaptation-Based Reconfiguration in the Presence of Actuator Failures and Saturation," *American Control Conference*, Jun. 2005. doi:10.1109/ACC.2005.1470366.

[31] Tjønnås, J., and Johansen, T., "Adaptive Control Allocation," *Automatica*, Vol. 44, No. 11, 2008, pp. 2754–2765. doi: 10.1016/j.automatica.2008.03.031.

[32] Falconi, G., and Holzapfel, F., "Adaptive Fault Tolerant Control Allocation for a Hexacopter System," *American Control Conference*, Jul. 2016. doi:10.1109/ACC.2016.7526736.

[33] Morelli, E., and Klein, V., *Aircraft System Identification: Theory and Practice*, 2nd ed., Sunflyte Enterprises, Williamsburg, VA, 2016, pp. 31–284.

[34] Morelli, E., "Real-Time Parameter Estimation in the Frequency Domain," *Journal of Guidance, Control, and Dynamics*, Vol. 23, No. 5, 2000, pp. 812–818. doi:10.2514/2.4642.

[35] Bryson, A., and Ho, Y., *Applied Optimal Control*, Hemisphere, 1975.

[36] Strang, G., *Linear Algebra and Its Applications*, 4th ed., Thomson Brooks/Cole, Belmont, CA, 2006, pp. 119–396.

[37] Åström, K., and Wittenmark, B., *Adaptive Control*, 2nd ed., Addison-Wesley Publishing Company, Reading, MA, 1995, pp. 137–146.

[38] Gelb, A., et al., *Applied Optimal Estimation*, The MIT Press, Cambridge, MA, 1974, pp. 107–119.

[39] Simon, D., *Optimal State Estimation*, John Wiley and Sons, Hoboken, NJ, 2006, pp. 73–74.

[40] McRuer, D., Ashkenas, I., and Graham, D., *Aircraft Dynamics and Automatic Control*, Princeton University Press, Princeton, NJ, 1973.

[41] Jordan, T., Langford, W., and Hill, J., "Airborne Subscale Transport Aircraft Research Testbed — Aircraft Model Development," *Guidance, Navigation, and Control Conference and Exhibit*, AIAA Paper 2005-6432, Aug. 2005. doi:10.2514/6.2005-6432.

[42] Barfield, A., "Multivariable Control Laws for the AFTI/F-16," Master's thesis, Air Force Institute of Technology, 1983.

[43] Nguyen, L., Ogburn, M., Gilbert, W., Kibler, K., Brown, P., and Deal, P., "Simulator Study of Stall/Post-Stall Characteristics of a Fighter Airplane With Relaxed Longitudinal Static Stability," NASA TP-1538, Dec. 1979.

[44] Anon., "Flying Qualities of Piloted Airplanes," Tech. Rep. MIL-F-8785C, Department of Defense, 1980.